PERFORMANCE ANALYSIS OF A GLRT IN LATE-TIME RADAR TARGET DETECTION

J. E. Mooney

Department of Electrical Engineering
200 Broun Hall
Auburn University
Alabama 36849, USA

Z. Ding

Department of Electrical and Computer Engineering
University of Iowa
Iowa City, IA 53346, USA

L. S. Riggs

Department of Electrical Engineering
200 Broun Hall
Auburn University
Alabama 36849, USA

1. INTRODUCTION

In the last two decades, a number of researchers have expended considerable effort researching techniques useful for radar target discrimination. Virtually all of these schemes attempt to extract some unique feature from a target's transient scattered field. Most of these techniques [1, 2] have utilized primarily the late-time portion of the transient response where the natural resonances of the target dominate. Because of the aspect independent characteristic of the natural resonances, these methods are an attractive approach to target discrimination. Recently, one of these schemes, the E-pulse technique, was applied to the early time component of the transient response with success [3]. Despite the highly aspect dependent behavior of the early-time region, this region is attractive since it contains the majority of the scattered energy. A common assumption implicit in all of these discrimination techniques is that a target has been detected and that it belongs to a family of possible candidates. In this paper, the issue of target detection will be addressed. Specifically, the objective is to detect a single target in Gaussian noise based on its transient scattered field return.

Previous work by Mooney et al. [1] demonstrated a robust target discrimination method using the late-time portion of the transient response and fundamental principles of detection and estimation theory, namely, hypothesis testing. As in the discrimination problem, the issue of target detection can be addressed by considering either the late-time or early-time portions of the scattered response. Building on the success of the approach presented in [1], a generalized likelihood ratio test is constructed using the singularity expansion method representation [4] of the late-time scattered field to decide whether a target is present or not.

To measure the performance of the GLRT, analytical expressions for the probability of detection and the probability of false alarm will be developed. These two parameters are normally plotted against one another for varying threshold levels to produce a curve known as the receiver operating characteristic (ROC). Results illustrating the ROC as a function of SNR for two different thin wire targets will be provided. The analytical results will be verified by generating the ROC curve through direct simulation. In addition, analytical and simulated results of a likelihood ratio test (LRT) will be given in order to provide an upper bound on performance. Finally, an analysis of how the modal content of the return affects the receiver operating characteristic will

be provided.

2. PROBLEM FORMULATION

The detection problem can be described in terms of a simple binary hypothesis test as follows:

$$
\begin{aligned}
H_1: &\quad y(t) = r(t) + n(t) \\
H_0: &\quad y(t) = n(t)
\end{aligned}
\tag{1}
$$

where $r(t)$ represents the scattered field from a target, and $n(t)$ is additive white Gaussian noise with zero mean and variance σ^2. Using the well known SEM representation of the late-time scattered field [4], the two hypotheses in (1) can be written as

$$
\begin{aligned}
H_1: &\quad y(t) = \sum_{i=1}^{N} a_i e^{s_i t} + n(t), \qquad t > T_L \\
H_0: &\quad y(t) = n(t)
\end{aligned}
\tag{2}
$$

where a_i and s_i denote the coupling coefficient and pole term, respectively, of the ith mode, N represents the total number of pole terms, and T_L is the beginning of the late-time period. The pole terms s_i are independent of aspect angle, but the coupling coefficients a_i and the late-time T_L are normally strong functions of the aspect angle.

For convenience, the various signals in (2) are represented by their uniform samples at the interval T_s as

$$
\mathbf{y} \equiv \begin{bmatrix} y(T_L) \\ y(T_L + T_s) \\ \vdots \end{bmatrix} ; \quad
\mathbf{b}_i \equiv \begin{bmatrix} e^{s_i T_L} \\ e^{s_i (T_L + T_s)} \\ \vdots \end{bmatrix} ; \quad
\mathbf{n} \equiv \begin{bmatrix} n(T_L) \\ n(T_L + T_s) \\ \vdots \end{bmatrix} .
$$

Hence, the sampled version of the two hypotheses in (2) become

$$
\begin{aligned}
H_1: &\quad \mathbf{y} = \mathbf{B}\mathbf{a} + \mathbf{n} \\
H_0: &\quad \mathbf{y} = \mathbf{n}
\end{aligned}
\tag{3}
$$

where the signal modes are represented by the matrix

$$
\mathbf{B} = [\, \mathbf{b}_1 \quad \mathbf{b}_2 \quad \cdots \quad \mathbf{b}_N \,],
$$

and the unknown coupling coefficients by the vector

$$\mathbf{a} = \begin{bmatrix} a_1 \\ a_2 \\ \vdots \\ a_N \end{bmatrix}$$

As noted previously, because of the aspect independent characteristic of the poles, the signal modes in $\mathbf{B}$ are assumed to be known. In contrast, the coupling coefficients in $\mathbf{a}$ are unknown because of their aspect dependent feature. Based on these assumptions and the two hypotheses given in (3), the objective is to develop a decision rule to determine whether or not a target is present. This decision rule will be based solely on the known signal modes $\mathbf{B}$ and measured return $\mathbf{y}$.

3. OVERVIEW OF THE LIKILIHOOD RATIO TEST

Before developing the decision rule for the case where the signal amplitudes are unknown, it is pertinent to develop and investigate a decision rule for the ideal case where all the signal parameters are known completely. The result of this analysis will provide an upper performance bound on any other decision rule which is based upon unknown signal parameters.

As shown in [5, 6], the optimum decision rule is a likelihood ratio test (LRT). The LRT consists of the ratio $L(\mathbf{y})$ of two likelihood functions which is tested against some threshold η as shown below

$$L(\mathbf{y}) = \frac{p(\mathbf{y}|\mathbf{a}, H_1)}{p(\mathbf{y}|\mathbf{a}, H_0)} \underset{H_0}{\overset{H_1}{\underset{<}{>}}} \eta. \tag{4}$$

The likelihood functions $p(\mathbf{y}|\mathbf{a}, H_1)$ and $p(\mathbf{y}|\mathbf{a}, H_0)$ are conditional probability density functions (pdf's) which can be generated by knowing the pdf of $\mathbf{n}$. Since the noise $\mathbf{n}$ has been characterized as being white and Gaussian with variance σ^2, the conditional pdf's $p(\mathbf{y}|\mathbf{a}, H_1)$ and $p(\mathbf{y}|\mathbf{a}, H_0)$ can be written as

$$p(\mathbf{y}|\mathbf{a}, H_1) = \frac{1}{(2\pi)^{q/2}\sigma^q} \exp\left[-\frac{1}{2\sigma^2}(\mathbf{y} - \mathbf{Ba})^H(\mathbf{y} - \mathbf{Ba})\right] \tag{5}$$

$$p(\mathbf{y}|H_0) = \frac{1}{(2\pi)^{q/2}\sigma^q} \exp\left[-\frac{1}{2\sigma^2}\mathbf{y}^H\mathbf{y}\right] \tag{6}$$

where q denotes the number of samples. Substituting (5) and (6) into (4) and letting $\mathbf{r} = \mathbf{Ba}$, the decision rule becomes

$$l(\mathbf{y}) = \mathbf{r}^T \mathbf{y} \underset{H_0}{\overset{H_1}{\gtrless}} \sigma^2 \ln \eta + \frac{1}{2} \|\mathbf{r}\|^2 \triangleq \gamma \tag{7}$$

where $\| \cdot \|$ denotes the Euclidean norm. Note that since $\mathbf{r}$ is real valued, the Hermitian operator has been replaced by the transpose operator.

Since the decision statistic $l(\mathbf{y})$ is Gaussian, the probability of false alarm is expressed as

$$P_F = \mathrm{erfc}\left(\frac{\gamma}{\sigma\|\mathbf{r}\|}\right) \tag{8}$$

where erfc is the complementary error function [7]. Similarly, the probability of detection is

$$P_D = \mathrm{erfc}\left(\frac{\gamma - \|\mathbf{r}\|^2}{\sigma\|\mathbf{r}\|}\right) \; . \tag{9}$$

4. THE GENERALIZED LIKELIHOOD RATIO TEST

As noted earlier, to use the LRT in (7), the noiseless return has to be known completely. Because of this omniscient characteristic of the LRT, it is not a very practical approach to the detection problem since a unique return is produced for each new target aspect. Specifically, the signal amplitudes $\mathbf{a}$ are highly dependent on the target orientation. A more practical approach is to develop a decision rule that treats $\mathbf{a}$ as an unknown parameter and utilizes only the aspect independent features of the signal model.

Since the LRT in (7) is not a uniformly most powerful (UMP) test, an alternative solution to determining a decision rule is to use the generalized likelihood ratio test (GLRT) [6]. The GLRT can be written in a form similar to the LRT as

$$\text{GLRT}: \qquad L_g(\mathbf{y}) = \frac{\max_{\mathbf{a}} p(\mathbf{y}|\mathbf{a}, H_1)}{\max_{\mathbf{a}} p(\mathbf{y}|\mathbf{a}, H_0)} \underset{H_0}{\overset{H_1}{\gtrless}} \eta \tag{10}$$

Maximizing the likelihood function

$$p(\mathbf{y}|\mathbf{a}, H_1) \propto \exp\left(-\frac{1}{2\sigma^2}(\mathbf{y} - \mathbf{Ba})^H(\mathbf{y} - \mathbf{Ba})\right)$$

is equivalent to minimizing $\|\mathbf{y} - \mathbf{Ba}\|^2$, hence yielding a least squares solution to $\mathbf{y} = \mathbf{Ba}$ as

$$\hat{\mathbf{a}}_{\max} = (\mathbf{B}^H\mathbf{B})^{-1}\mathbf{B}^H\mathbf{y}. \tag{11}$$

Substituting the least squares solution into (10) and taking the natural logarithm of both sides, one obtains after some manipulation

$$l_g(\mathbf{y}) \triangleq \ln L_g(\mathbf{y}) = \mathbf{y}^H\mathbf{P}\mathbf{y} \underset{H_0}{\overset{H_1}{\gtrless}} 2\sigma^2 \ln \eta \triangleq \gamma_g \tag{12}$$

The $q \times q$ matrix $\mathbf{P} = \mathbf{B}(\mathbf{B}^H\mathbf{B})^{-1}\mathbf{B}^H$ is known as the projection matrix and has the following useful properties [8]:

  A. $\mathbf{P}$ is symmetric.
  B. $\mathbf{P}$ is idempotent $(\mathbf{P}^2 = \mathbf{P})$.
  C. The eigenvalues of $\mathbf{P}$ are either 1 or 0.
  D. The rank of $\mathbf{P}$ is equal to the number of poles N used in the SEM representation of the far scattered field.

To determine P_F and P_D, the distribution of the decision statistic $l_g(\mathbf{y})$ needs to be known. The decision statistic has the quadratic form $\mathbf{y}^H\mathbf{P}\mathbf{y}$ and represents a weighted sum of squared Gaussian random variables. Under certain conditions, such a sum has a non-central χ^2 distribution [9]. Its distribution is denoted $\chi'^2(\nu, \theta)$ where the constant ν is called the number of degrees of freedom and θ is the eccentricity. In statistical literature, the eccentricity is also referred to as the non-centrality parameter [10]. The probability density function of a random variable x with a non-central χ^2 distribution with ν degrees of freedom and eccentricity[1] θ is given by [10]

$$p(x; \nu, \theta) = e^{-\frac{1}{2}\theta} \sum_{k=0}^{\infty} \frac{\left(\frac{1}{2}\theta\right)^k x^{\left(\frac{1}{2}\nu+k-1\right)} e^{-\frac{1}{2}x}}{k! 2^{\left(\frac{1}{2}\nu+k\right)} \Gamma\left(\frac{1}{2}\nu + k\right)}, \qquad x > 0 \tag{13}$$

---

[1]   In some statistical literature, the eccentricity is defined as $\lambda = \frac{1}{2}\theta$ [11].

The cumulative distribution function (c.d.f.) of the non-central χ^2 random variable is defined as

$$F(x; \nu, \theta) = P\left\{\chi'^2(\nu, \theta) \leq x\right\} = \int_{-\infty}^{x} p(\tau; \nu, \theta)d\tau$$

$$= e^{-\frac{1}{2}\theta} \sum_{k=0}^{\infty} \frac{\left(\frac{1}{2}\theta\right)^k}{k!2^{\left(\frac{1}{2}\nu+k\right)}\Gamma\left(\frac{1}{2}\nu + k\right)} \int_{0}^{x} \tau^{\left(\frac{1}{2}\nu+k-1\right)}e^{-\frac{1}{2}\tau}d\tau \quad (14)$$

Computing the c.d.f. of $\chi'^2(\nu, \theta)$ is not a trivial task since it involves computing the incomplete gamma function within an infinite sum. Fortunately, several researchers [12, 13] have developed sophisticated and accurate algorithms for numerically evaluating the c.d.f. of the non-central χ^2 distribution.

An extremely important theorem concerning the distribution of the quadratic form $\mathbf{y}^H \mathbf{P} \mathbf{y}$ is developed by Papoulis [9] and is stated as follows:

If $\mathbf{y}$ is distributed as $N(\boldsymbol{\mu_y}, \mathbf{I})$ then $\mathbf{y}^H \mathbf{P} \mathbf{y}$ is distributed as $\chi'^2(N, \boldsymbol{\mu_y}^H \mathbf{P} \boldsymbol{\mu_y})$ if and only if $\mathbf{P}$ is idempotent of rank N.

This theorem is applicable to the decision statistic $l_g(\mathbf{y})$ because of the properties of the projection matrix. Letting $\mathbf{y} = \sigma \mathbf{z}$ where $\mathbf{z}$ is distributed as $N(\boldsymbol{\mu_y}/\sigma, \mathbf{I})$, the decision statistic can be now written as

$$l_g(\mathbf{y}) = \mathbf{y}^H \mathbf{P} \mathbf{y} = \sigma^2 \mathbf{z}^H \mathbf{P} \mathbf{z} \mathop{\gtrless}_{H_0}^{H_1} \gamma_g \quad (15)$$

Using the theorem [9], the decision statistic $l_g(\mathbf{y})$ is distributed as

$$l_g(\mathbf{y}) \sim \frac{1}{\sigma^2}\chi'^2\left(N, \frac{1}{\sigma^2}\boldsymbol{\mu_y}\mathbf{P}\boldsymbol{\mu_y}\right). \quad (16)$$

Knowing the distribution of $l_g(\mathbf{y})$, the probability of false alarm and the probability of detection can be computed. Under H_0, $\boldsymbol{\mu_y} = \mathbf{0}$, and $l_g(\mathbf{y})$ is distributed as

$$l_g(\mathbf{y}) \sim \frac{1}{\sigma^2}\chi'^2(N, 0). \quad (17)$$

Thus, the probability of false alarm can be expressed in terms of the non-central χ^2 c.d.f. as

$$
\begin{aligned}
P_F &= P\{l_g(\mathbf{y})|H_0 > \gamma_g\} \\
&= 1 - P\{l_g(\mathbf{y})|H_0 \le \gamma_g\} \\
&= 1 - P\left\{\sigma^2 \mathbf{z}^H \mathbf{P} \mathbf{z}|H_0 \le \gamma_g\right\} \\
&= 1 - P\left\{\chi'^2(N, 0) \le \frac{\gamma_g}{\sigma^2}\right\} \\
&= 1 - F(2\ln\eta; N, 0).
\end{aligned}
\tag{18}
$$

Similarly, under H_1, $\boldsymbol{\mu_y} = \mathbf{Ba}$, and $l_g(\mathbf{y})$ is distributed as

$$
l_g(\mathbf{y}) \sim \frac{1}{\sigma^2}\chi'^2\left(N, \frac{\|\mathbf{Ba}\|^2}{\sigma^2}\right).
\tag{19}
$$

Hence, the probability of detection can be written in terms of the cumulative distribution function as

$$
P_D = 1 - F\left(2\ln\eta; N, \frac{\|\mathbf{Ba}\|^2}{\sigma^2}\right).
\tag{20}
$$

Recall that $\mathbf{Ba}$ represents the late-time backscattered return from a target. Hence, the ratio $\|\mathbf{Ba}\|^2/\sigma^2$ is the ratio of the late-time signal energy to the average noise power.

The calculation of P_F and P_D are illustrated in Fig. 1. Since the eccentricity of $l_g(\mathbf{y})$ under H_1 is inversely proportional to the noise power, the two densities in Fig. 1 can be separated by simply decreasing σ^2. Thus, for small σ^2, certain thresholds exist where a high probability of detection can be maintained while simultaneously keeping the probability of false alarm low.

5. ANALYTICAL AND SIMULATED RESULTS

In this section, results demonstrating the performance of the GLRT are provided. The performance results of the GLRT are analyzed by plotting the receiver operating characteristic (ROC). The ROC of the GLRT for two different targets are investigated under varying SNR and aspect angle. The ROC of the GLRT is developed analytically using (18) and (20) from the previous section. To verify the analytical results, the ROC is generated directly through simulation. As a basis
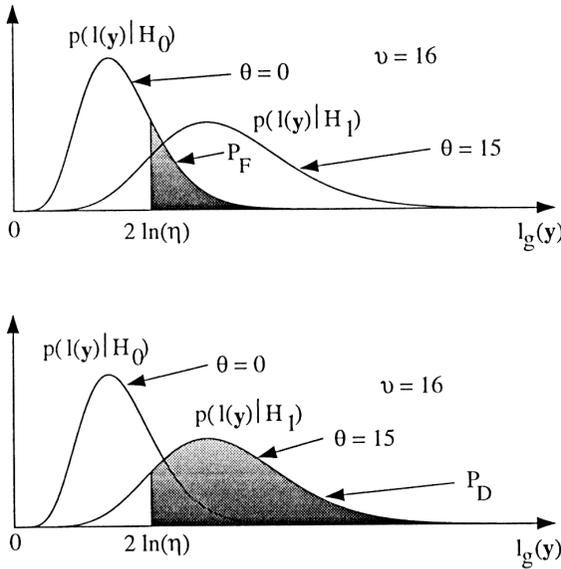
Figure 1. The probability densities of $l_g(\mathbf{y})$ under hypotheses H_1 and H_0. The calculation of P_F and P_D are also shown.

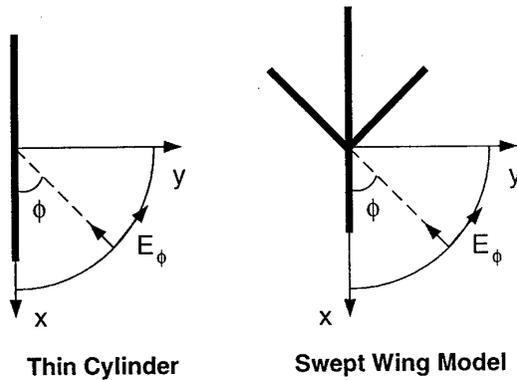Thin Cylinder   Swept Wing Model

Figure 2. Illustrations of the thin cylinder and the $45°$ swept wing aircraft model.

for comparison, the GLRT results are compared with the analytical and simulated ROC's of the LRT.

The two targets to be studied are the thin cylinder and the $45°$ swept wing aircraft model. Both of these targets are illustrated in

Fig. 2. The thin cylinder, which is oriented along the x-axis and centered at the origin, has a length of 1 m and a radius of 0.005 m. The swept wing model is constructed of similar thin wires having a length-to-radius ratio of 200. The fuselage is 1 m in length. The section of the fuselage forward of the wings has a length of 1/3 m. The section aft of the wings is of length 2/3 m. Both wings are swept back 45° from the normal to the fuselage and have a length of 1/2 m. The aspect angle ϕ, as illustrated in Fig. 2 is defined to be in the plane of the target and is measured from the x-axis.

The scattering data used in generating the analytical results as well as the simulated results are the theoretical impulse responses of the two targets shown in Fig. 2. These responses were obtained using the SEM which was cast into numerical form via the method of moments [14]. The poles that were used in obtaining the backscattered field from each target are listed in Table 1. The first eight complex conjugate pole pairs were used in computing the backscattered field impulse response of the 1 m thin cylinder. In order to ensure that the same bandwidth was used among each of the two targets, it was necessary to use the first fifteen conjugate poles pairs to compute the impulse response of the 45° swept wing aircraft model. It should be noted here that the impulse responses for all targets were computed using a Class I coupling coefficient; thus, the early time portion of the responses are inaccurate [15, 16]. The beginning of the late-time period T_L is dependent on the aspect angle of the target. Since the aspect angle is assumed to be unknown in this analysis, T_L is calculated as twice the maximum one-way transit time of the target. Both the thin cylinder and the swept wing model have a maximum linear dimension of 1 m; hence, $T_L = 2/c$ for both targets where c denotes the speed of light.

5.1 Analytical Results

As noted earlier, the ROC of the GLRT is generated by direct implementation of (18) and (20). The computation of the probability of detection is directly dependent on the SNR since the eccentricity parameter of the non-central χ^2 distribution is inversely proportional to the noise power. To determine the ROC for a specified SNR, the average power of the noise-free backscattered return $r(t)$ from a target

| $\frac{S_{m,n}}{c}$	Thin Cylinder		45° Swept Wing	
m, n	Real	Imag.	Real	Imag.
1,1	−0.2574	± 2.8743	−0.1142	± 2.6857
1,2	−0.3792	± 5.9329	−0.1748	± 3.0526
1,3	−0.4660	± 9.0117	−0.3215	± 3.6096
1,4	−0.5353	± 12.0955	−0.4772	± 6.6065
1,5	−0.5935	± 15.1775	−0.4059	± 7.9230
1,6	−0.6436	± 18.2533	−0.6182	± 9.3581
1,7	−0.6870	± 21.3193	−0.5594	± 11.0463
1,8	−0.7244	± 24.3726	−0.5560	± 12.0588
1,9	* * * * *	* * * **	−0.5882	± 14.8595
1,10	* * * * *	* * * **	−0.8985	± 15.4000
1,11	* * * * *	* * * **	−0.6356	± 16.4076
1,12	* * * * *	* * * **	−0.7755	± 18.7524
1,13	* * * * *	* * * **	−0.6201	± 21.1990
1,14	* * * * *	* * * **	−0.9542	± 21.5145
1,15	* * * * *	* * * **	−0.7550	± 22.34780

Table 1. The natural frequencies of the two targets used in the numerical examples.

must be computed. The average power of $r(t)$ is defined as

$$P_{sig} = \frac{1}{T} \int_0^T r^2(t)dt \tag{21}$$

Once P_{sig} is known, the average noise power σ^2 can be calculated for a specified SNR (in dB). For the backscattered returns used in these results, the end time of the integration is arbitrarily chosen to be 50 ns. Figure 3 shows the backscattered response from the thin cylinder at an aspect angle $\phi = 75°$ and an SNR of -10 dB.

With the average noise power determined, the computation of P_F and P_D for the GLRT follow directly from (18) and (20), respectively. The ROC is generated by repeatedly solving these two equations over a range of thresholds. The beginning threshold value is selected low enough such that both P_F and P_D are one. The final threshold value is set large enough so that both P_F and P_D are zero. As discussed earlier, solving for P_D and P_F is numerically challenging because of
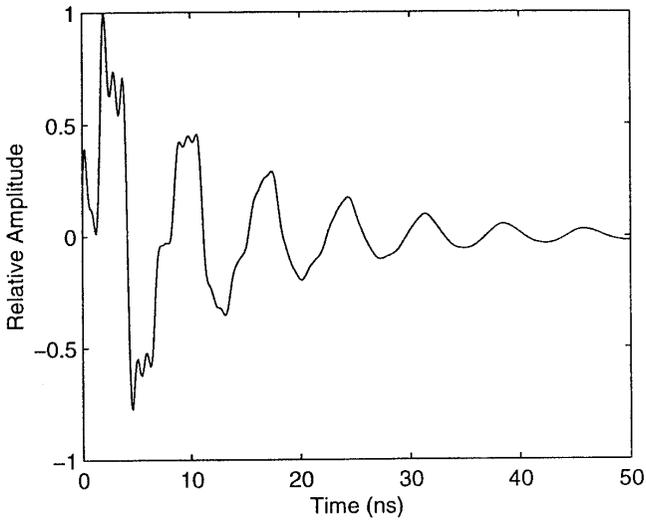
(a) The noiseless transient return.
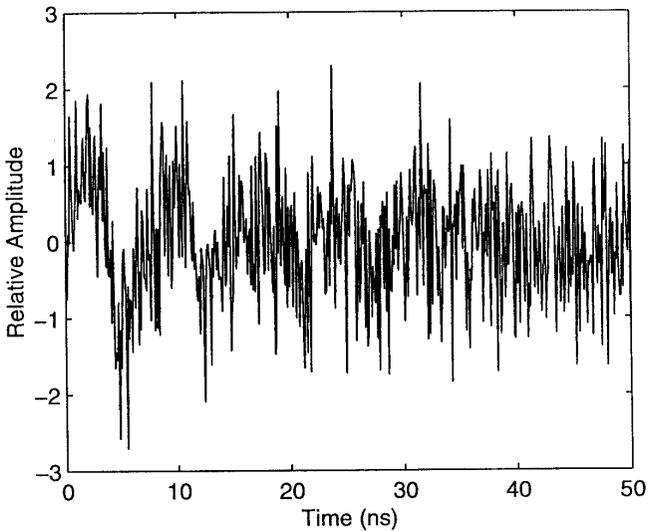
(b) The transient return with a SNR of $-10\,\mathrm{dB}$.

Figure 3. The transient return from the thin cylinder at $\phi = 75°$.

the presence of the non-central χ^2 cumulative distribution function. Fortunately, a number of researchers have developed algorithms to efficiently and accurately compute the $\chi'^2(\nu, \theta)$ c.d.f. The algorithm by Ding [12] was employed to generate the ROC of the GLRT. The ROC of the LRT is developed the same way as the ROC of the GLRT, but involves repeated calculation of (8) and (9) over a range of thresholds.

5.2 Simulation Results

As a way of verifying the analytical results, the ROC of the GLRT is developed through direct simulation. The simulation process involves using the scattering data directly in the GLRT. To generate a simulated version of the probability of detection and a simulated version of the probability of false alarm, two separate experiments are carried out. These simulated versions of the probability of detection and false alarm are better termed as detection and false alarm rates, respectively.

The experiment to determine the detection rate consists of first adding white Gaussian noise to the return $r(t)$. The average noise power is adjusted accordingly to yield a specified SNR. Using the corrupted return, a value for the decision statistic in (12) is computed and compared with the threshold γ_g. If the value of the decision statistic exceeds the threshold, then a detection is declared and tallied. This process is repeated 1000 times at *each* threshold to yield a detection rate.

In the second experiment, white Gaussian noise with the same noise power σ^2 as in the first experiment is generated. Using the noise as the return, the decision statistic in (12) is calculated and compared with the threshold γ_g. If the value of the decision statistic exceeds the threshold, a false alarm is declared and tallied. As in the first experiment, this process is repeated 1000 times at *each* threshold to yield a false alarm rate.

The detection and false alarm rates obtained by repeating these experiments over a range of thresholds are used to produce a simulated ROC for the GLRT. The same simulation process is also carried out using (7) to develop a simulated ROC for the LRT.

5.3 Results

The receiver operating characteristics of the GLRT and LRT are shown in Figs. 4–9 for the thin cylinder and the $45°$ swept wing aircraft
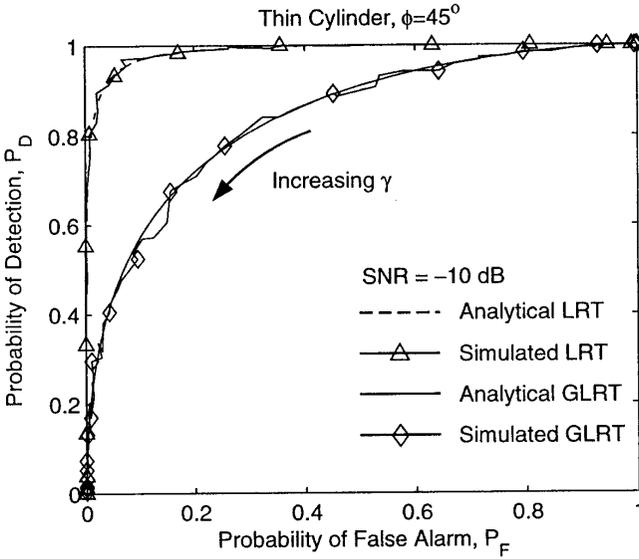
Figure 4. The receiver operating characteristic for the thin dipole at $\phi = 45°$ and SNR of -10 dB.
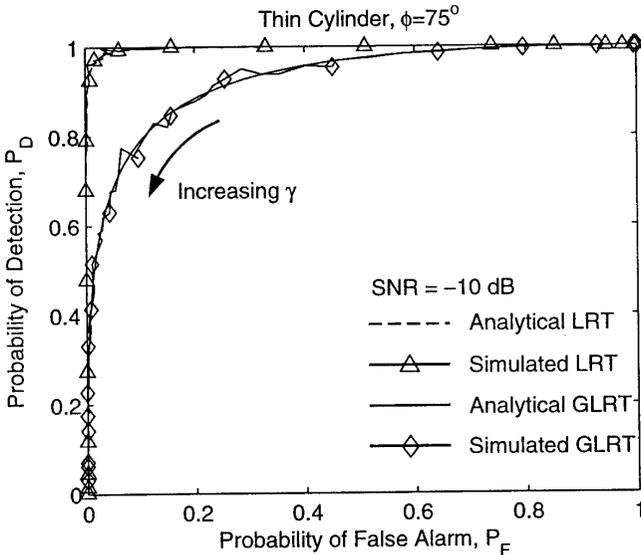

Figure 5. The receiver operating characteristic of the GLRT and LRT for the thin dipole at $\phi = 75°$ and SNR of -10 dB.

model. Figures 4 and 5 display the simulated and analytical ROC's of the GLRT and LRT for the thin cylinder under varying SNR conditions and aspect angles. Figures 6 and 7 provide a similar analysis for the ROC for the swept wing aircraft model. Finally, the effect the number of poles has on the ROC is analyzed in Figs. 8 and 9.

Before examining the results, a brief discussion of some of the fundamental properties of ROC's is pertinent. These properties apply only to ROC's generated from continuous likelihood ratio tests as is the case here [6]. The first property pertains to the shape of the ROC. The shape of all ROC's is concave downward. Furthermore, every ROC contains the points $(P_F = 0, \ P_D = 0)$ and $(P_F = 1, \ P_D = 1)$. The lower bound on a ROC is a line (the chance diagonal) connecting these points, i.e., $P_F = P_D$. In contrast, an optimum ROC is one where the probability of detection is one for nearly all thresholds.

Figures 4 and 5 show the ROC of the thin cylinder for an SNR of $-10\,\mathrm{dB}$. The only difference between these two figures is the aspect angle. In Fig. 4, where the aspect angle is $45°$, both the simulated and analytical version of the ROC agree well with each other. As expected, the performance of the LRT exceeds the performance of the GLRT. These same observations can be made in Fig. 5 where the aspect angle is $75°$. However, when comparing Figs. 4 and 5, one observes that the performance of the GLRT and LRT is slightly better in Fig. 5 than in Fig. 4. The primary reason for this slight gain in performance is that there is more signal content at $\phi = 75°$ than at $\phi = 45°$. Furthermore, as seen in (20), the probability of detection is very much dependent on the late-time energy of the return. In general, as the aspect angle of the incident waveform illuminating the thin cylinder is reduced, the energy in the late-time portion of the return decreases. A decrease in the late-time energy of the signal decreases the eccentricity of the distribution used to compute P_D. Consequently, the underlying distributions of P_F and P_D become less distinct, and the ROC moves in the direction of the chance diagonal.

Figure 6 and 7 display the ROC for the $45°$ swept wing model under the same conditions that were used to analyze the ROC of the thin cylinder. By inspecting these results, we see many of the same features and trends that were observed in the results for the thin cylinder. The primary features include excellent agreement between the simulated and analytical results for the LRT ROC and GLRT ROC and a degradation in performance with decreasing SNR. The effect of aspect angle
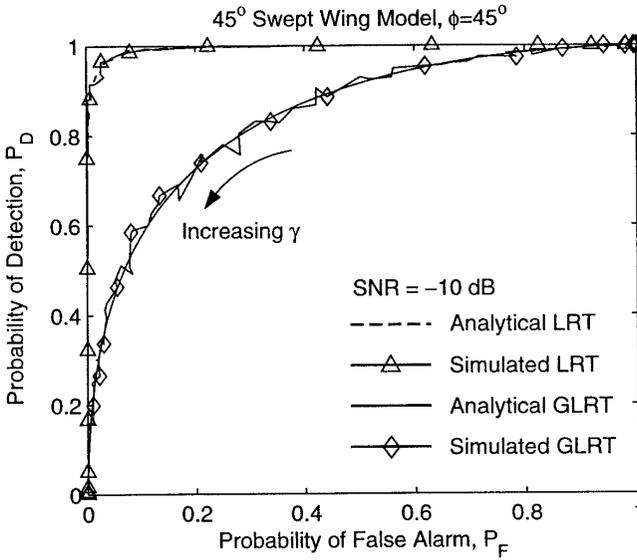
45° Swept Wing Model, φ=45°

Increasing γ

SNR = −10 dB
- - - - - Analytical LRT
——△—— Simulated LRT
——— Analytical GLRT
——◇—— Simulated GLRT

Probability of Detection, P_D

Probability of False Alarm, P_F

Figure 6. The receiver operating characteristic of the GLRT and LRT for the $45°$ swept wing aircraft model at $\phi = 45°$ and SNR of -10 dB.
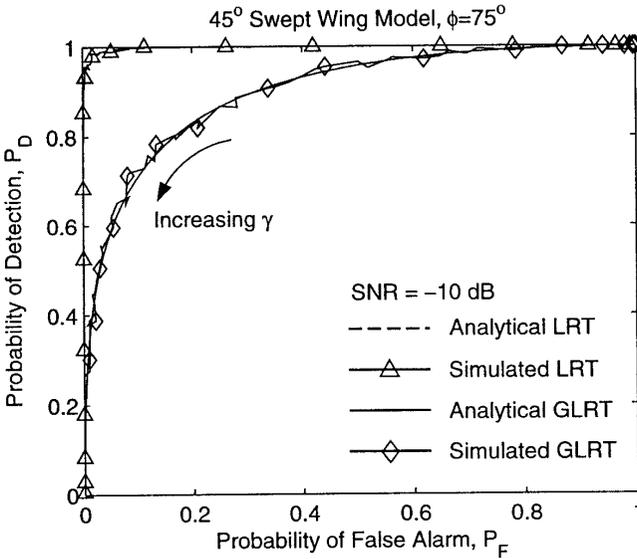
45° Swept Wing Model, φ=75°

Increasing γ

SNR = −10 dB
- - - - - Analytical LRT
——△—— Simulated LRT
——— Analytical GLRT
——◇—— Simulated GLRT

Probability of Detection, P_D

Probability of False Alarm, P_F

Figure 7. The receiver operating characteristic of the GLRT and LRT for the $45°$ swept wing aircraft model at $\phi = 75°$ and SNR of -10 dB.
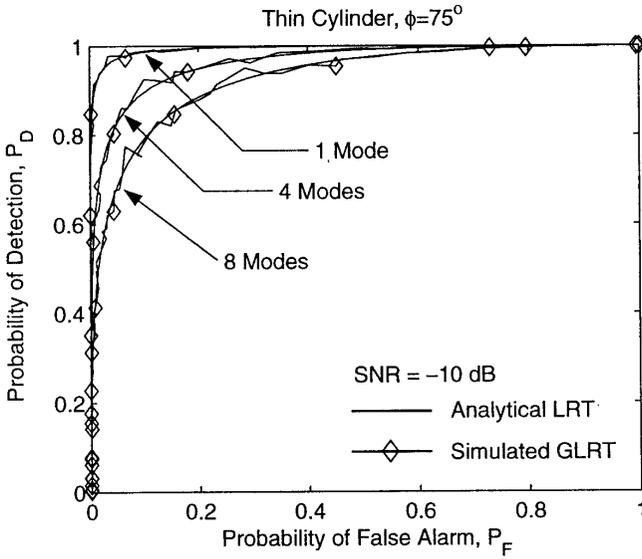
Figure 8. The receiver operating characteristic of the GLRT for the thin cylinder using 1, 4, and 8 pole-pairs.
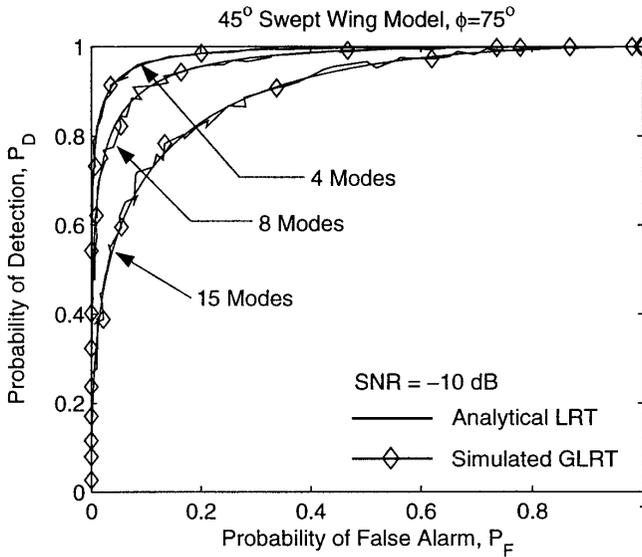

Figure 9. The receiver operating characteristic of the GLRT and LRT for the 45° swept wing aircraft model using 4, 8, and 15 pole-pairs.

on the ROC is also noticeable. In general, for a given SNR, the ROC improves as the aspect angle approaches broadside illumination.

Figure 8 and 9 illustrate the effect the number of pole-pairs (modes) has on the ROC of both the thin cylinder and the swept wing model. In Fig. 8, the ROC of the GLRT is shown for the thin cylinder using only the fundamental mode, the first 4 modes, and the first 8 modes. In constructing the ROC's in Fig. 8, the returns from the thin cylinder were recomputed to represent the appropriate modal content. As one can observe, decreasing the modal content improves the ROC. This observation is also made in Fig. 9 where several ROC's are shown for the swept wing model. In the analysis of this target, the first 4, 8, and 15 modes were used. Based on the results presented in Figs. 8 and 9, one can conclude that decreasing the number of poles, or equivalently, the bandwidth of the detection system, improves the ROC. This result is predicted by the dependency of the density functions, specifically the degrees of freedom, used to calculate P_F and P_D on the modal content of the return.

6. CONCLUSIONS

In this paper, the problem of detecting a single target based on its natural resonances was studied. Beginning with the SEM representation of the scattered field and with simple binary hypothesis testing, a generalized likelihood ratio (GLRT) test was developed to determine whether or not a target is present. To measure the performance of the GLRT, analytical expressions for the probability of detection and for the probability of false alarm were developed.

Results illustrating the performance of the GLRT were presented for two simple thin wire targets. These results, known as receiver operating characteristics (ROC's), consisted of plotting the probability of detection versus the probability of false alarm. For each target, ROC's were provided which demonstrated the performance of the GLRT for different aspect angles. The ROC's generated from the analytical expressions for P_F and P_D were verified through direct simulation.

REFERENCES

1. Mooney, J. E., Z. Ding, and L. S. Riggs, "Robust target identification in white Gaussian noise for ultra-wideband radar systems," *IEEE Trans. Antennas Propagation,* Vol. AP-46, 1817–1823, Dec. 1998.

2. Baum, C. E., E. J. Rothwell, K. M. Chen, and D. P. Nyquist, "The singularity expansion method and its application to target identification," in *Proceedings of the IEEE,* Vol. 79, 1481–1492, Oct. 1991.

3. Rothwell, E. J., K. M. Chen, D. P. Nyquist, P. Ilavarasan, J. E. Ross, R. Bebermeyer, and Q. Li, "A general E-pulse scheme arising from the dual early-time/late-time behavior of radar scatterers," *IEEE Trans. Antennas Propagat.,* Vol. AP-42, 1336–1341, Sept. 1994.

4. Baum, C. E., "On the singularity expansion method for the solution of electromagnetic interaction problems," Interaction Note 88, Air Force Weapons Lab, 1971.

5. Srinath, M., P. K. Rajasekaran, and R. Viswanathan, *Introduction to Statistical Signal Processing with Applications,* Prentice Hall, 1996.

6. Van Trees, H. L., *Detection, Estimation, and Modulation Theory Part I,* John Wiley & Sons, 1967.

7. Abramovitz, M., and I. A. Stegun, *Handbook of Mathematical Functions,* U.S. Government Printing Office, Washington, D.C.: National Bureau of Standards, 1964.

8. Kay, S. M., *Fundamentals of Statistical Signal Processing: Estimation Theory,* Prentice Hall, 1983.

9. Papoulis, A., *Probability and Statistics,* Prentice Hall, 1990.

10. Johnson, N. L., S. Kotz, and N. Balakrishnan, *Continuous Univariate Distributions,* Vol. 2, Ch. 29, 433–479, John Wiley & Sons, 1995.

11. Searle, S. R., *Linear Models,* Ch. 2, 54–64, John Wiley & Sons, 1971.

12. Ding, C. G., "Algorithm AS 275: Computing the non-central χ^2 distribution function," *Applied Statistics,* Vol. 41, 478–482, 1992.

13. Ashour, S. K., and A. I. Abdel-Samad, "On the computation of non-central χ^2 distribution function," *Communications in Statistics-Simulation and Computation,* Vol. 19, 1279–1291, 1990.

14. Harrington, R. F., *Field Computation by Moment Methods,* IEEE Press, 1993.

15. Richards, M. A., "SEM representation of the early and late time fields scattered from wire targets," *IEEE Trans. Antennas Propagation,* Vol. AP-42, 564–566, 1994.

16. Baum, C. E., "Representation of surface current density and far
     scattering in EEM and SEM with entire functions," Interaction
     Note 486, Phillips Laboratory, Feb. 1992; Ch. 13, 273–316, in
     P. P. Delsanto and A. W. Saenz, eds., *New Perspectives on Prob-
     lems in Classical and Quantum Physics, Part II: Acoustic Prop-
     agation and Scattering, Electromagnetic Scattering*, Gordon and
     Breach, 1998.
17. Johnson, N. L., S. Kotz, and N. Balakrishnan, *Continuous Uni-
     variate Distributions,* Vol. 1, Ch. 18, 415–493, John Wiley &
     Sons, 1995.
18. Brillinger, D. R., "The analysis of time series collected in an ex-
     perimental design," in *Multivariate Analysis-III,* P. R. Krishnaiah
     (Ed.) 241–256, Academic Press, 1973.